ADVANCED MATERIALS
www.advmat.de

# Multicolor Photonic Pigments for Rotation-Asymmetric Mechanochromic Devices

*Zhiwei Li, Xiaojing Wang, Lili Han, Chenhui Zhu, Huolin Xin, and Yadong Yin**

**Photonic crystals are extensively explored to replace inorganic pigments and organic dyes as coloring elements in printing, painting, sensing, and anti-counterfeiting due to their brilliant structural colors, chemical stability, and environmental friendliness. However, most existing photonic-crystal-based pigments can only display monochromatic colors once made, and generating multicolors has to start with designing different building blocks. Here, a novel photonic pigment featuring highly tunable structural colors in the entire visible spectrum, made by the magnetic assembly of monodisperse nanorods into body-centered-tetragonal photonic crystals, is reported. Their prominent magnetic and crystal anisotropy makes it efficient to generate multicolors using one photonic pigment by magnetically controlling the crystal orientation. Further, the combination of angle-dependent diffraction and magnetic orientation control enables the design of rotation-asymmetric photonic films that display distinct patterns and encrypted information in response to rotation. The efficient multicolor generation through precise orientational control makes this novel photonic pigment promising in developing high-performance structural-colored materials and optical devices.**

## 1. Introduction

Photonic crystals are structures with periodic low and high refractive indexes.[1] Their most compelling feature is optical diffractions at a wavelength determined by surrounding dielectrics and the periodicity and orientation of their lattices.[2] The constructive interference of light results in brilliant structural colors.[3–5] Comparing with the classic top-down fabrication methods,[6] the bottom-up approaches involving colloidal self-assembly have been extensively studied because of the widely accessible building blocks and the ease of assembling them into diverse secondary structures.[7] The combination of low-cost self-assembly with optical properties of solid particles makes colloidal photonic crystals promising alternatives to conventional pigments and organic dyes.[8,9] Their structural colors are brighter and much more stable than organic dyes because the optical diffraction originates from the periodic arrangement of materials that do not photobleach. In principle, the colors can be tuned by controlling crystal periodicity and orientation, thereby providing a widely accessible range of colors using a single material.[10] To this end, many methods have been developed to achieve delicate control over crystal symmetry and periodicity, aiming to generate structural colors to meet the requirements of practical applications.[11]

A few prerequisites exist in using photonic crystals as pigments in place of organic dyes.[8,12] First, their structural colors should be widely tunable while maintaining stability in daily use. Second, their further advancement to practical applications, particularly in integrated optical devices and miniature photonic chips, requires easy access to patterned photonic crystals with highly controllable colors and domains.[13] To this end, the self-assembly of colloidal crystal arrays from nanospheres has been extensively studied, with many methods being developed for creating colloidal photonic pigments, including capillary-driven colloidal assembly,[14] emulsion-assisted assembly of microbeads,[10,15] and diverse coating methods.[16] Besides, a few advanced printing techniques are also available to pattern photonic crystals into devices,[17] such as inkjet printing[18] and 3D copolymers deposition.[19] Most of these photonic crystals comprise close-packed nanospheres so that their structural colors are largely determined by particle size.[20] It therefore requires precise size control to produce different colors and then, color mixing for generating multiple colors.[21] Another disadvantage associated with the highly symmetric close-packing of either face-centered cubic or less often hexagonal-phase pigments is the small tunability of the structural colors. This limitation adds challenges to their use in developing emerging optical materials and devices for advanced applications such as information encryption, anti-counterfeiting, and sensing, where responsive photonic pigments are highly desirable for displaying hidden information or sensing target molecules.[3,22] Assembling anisotropic colloids into photonic crystals is an efficient way to break the typical lattice symmetry resulting from

Z. Li, X. Wang, Y. Yin
Department of Chemistry
University of California, Riverside
Riverside, CA 92521, USA
E-mail: yadong.yin@ucr.edu
L. Han, H. Xin
Department of Physics and Astronomy
University of California-Irvine
Irvine, CA 92697, USA
C. Zhu
Advanced Light Source
Lawrence Berkeley National Laboratory
Berkeley, CA 94720, USA
The ORCID identification number(s) for the author(s) of this article can be found under https://doi.org/10.1002/adma.202107398.

**DOI: 10.1002/adma.202107398**

 

the assembly of spherical building blocks.[23] A great benefit in this regard is that many colloidal syntheses have been developed to prepare nanostructures with anisotropic shapes and heterogeneous chemical compositions.[24] And, the easy access to these monodisperse building blocks makes it possible to prepare photonic crystals exhibiting multiple colors. For example, nanorods and nanodiscs can be assembled into photonic crystals with reduced crystal symmetry and orientation-dependent structural colors.[4,13,25] However, advancing these materials toward practical applications still requires solving several critical technical challenges, including transforming the non-close-contacted photonic crystals into pigments and precise orientation control for multicolor generation. In this work, we report the development of a class of high-quality photonic pigments that can display stable, bright, and precisely tunable structural colors. These novel photonic pigments, produced by magnetic assembly of uniform $Fe_3O_4$@$SiO_2$ nanorods in colloidal dispersion followed by sol–gel fixation, feature a body-centered-tetragonal lattice and a ribbon-like overall shape. The high anisotropy of the crystal structure combined with the magnetic shape anisotropy of the building blocks allows the generation of multiple colors by simply changing the direction of the applied magnetic field. By taking advantage of the unique optical properties of the tetragonal crystals, we further demonstrate the development of rotation-asymmetric photonic devices that can display color switching or distinct images in response to mechanical rotation.

## 2. Results and Discussion

### 2.1. Magnetic Assembly of Tetragonal Photonic Pigments

Uniform magnetic nanorods were prepared by synthesizing FeOOH nanorods (320 nm in length and 70 nm in width) using a hydrolysis reaction, coating them with a layer of silica of controllable thickness, and then reducing them to magnetic $Fe_3O_4$ phase with shape preservation by the silica shells.[26] The transmission electron microscopy (TEM) images in Figure S1a,b, Supporting Information, demonstrate the excellent uniformity of FeOOH and $Fe_3O_4$@$SiO_2$ nanorods. The digital pictures in **Figure 1**a depict the assembly of monodisperse nanorods under a permanent magnet and the precipitation of resulting large crystals driven by magnetic packing force.[27] Under the applied magnetic field, the sparkling crystals exhibit green color. Under a dark-field optical microscope, the ribbon-like crystal exhibits

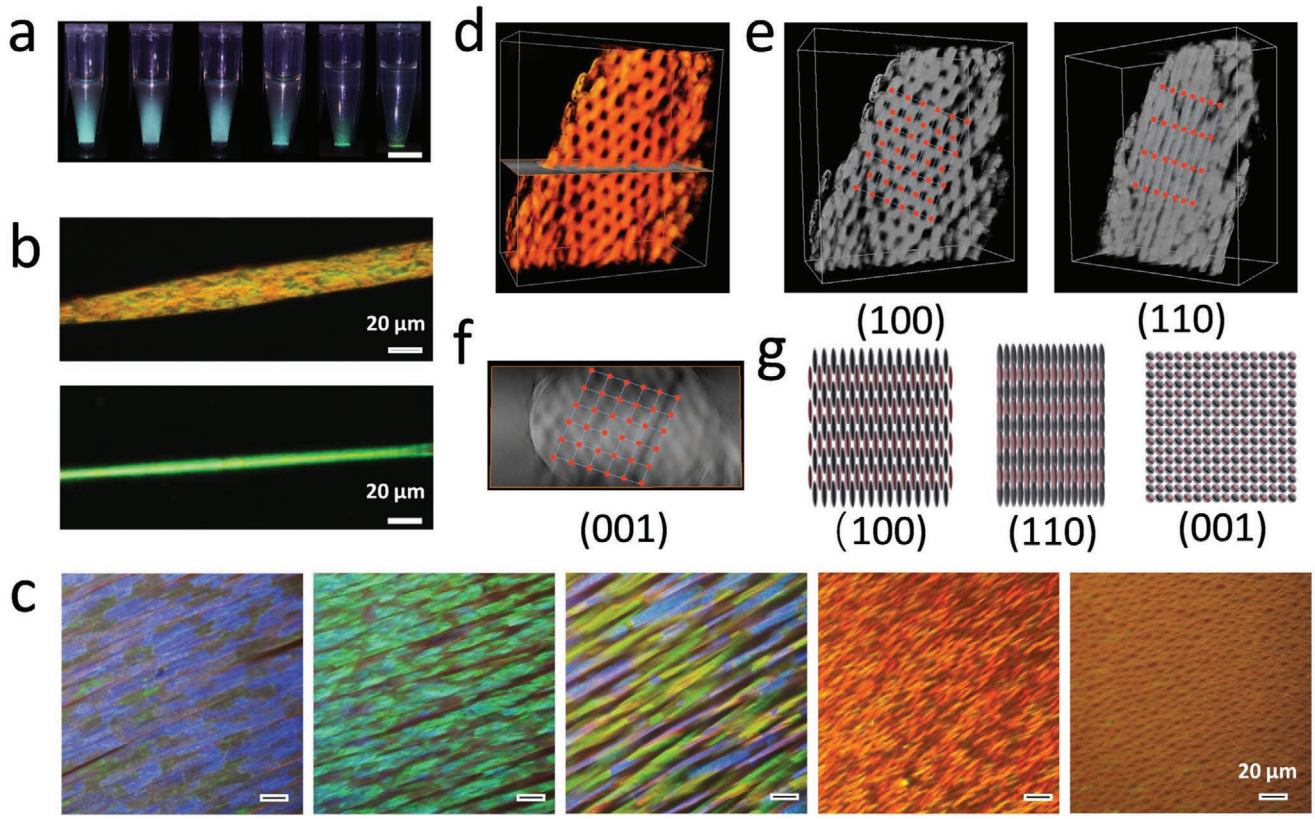


**Figure 1.** a) Digital pictures showing the self-assembly of $Fe_3O_4$@$SiO_2$ nanorods in the mixture of water and ethanol under a vertical magnetic field. Scale bar: 2 mm. b) Dark-field optical microscopy images of the assembled photonic crystals with exposed (100) and (110) facets shown in the top and bottom panels, respectively. c) Dark-field optical microscopy images of the self-assembled photonic crystal in magnetic fields with varying directions from horizontal (left) to vertical (right). d) 3D rendering of TEM tomography of a photonic crystal. e) 3D rendering of the same crystal with two different exposed facets as indicated, leading to two typical projection patterns. f) A horizontal cross-section of the reconstructed photonic crystal with exposed (001) facets, which reveals the rod packing along <001> crystal direction. g) Schematic illustrations of the projections of the photonic crystal with exposed (100), (110), and (001) facets, demonstrating the rod packing along the <100>, <110>, and <001> crystal directions, respectively.

 

distinct structural colors at two typical orientations because of the different periodicity along these two crystal directions (Figure 1b). The uniform yellow (top panel in Figure 1b) and green colors (bottom panel in Figure 1b) from the ribbon crystal surface and edge suggest the formation of 3D structures. Besides, their structural colors can be readily tuned by the magnetic field direction: changing the field direction from horizontal to vertical leads to a continuous redshift of the perceived colors from blue to green, yellow, and red (Figure 1c).

Stable photonic pigments were formed by fixing the assembled colloidal crystals using sol–gel chemistry, involving the hydrolysis of tetraethoxysilane to produce colloidal silica to glue the adjacent rods together (Figure 1a).[28] An additional silica layer is coated on the assembled crystals in synchrony with the crystal fixation. This sequence of events produces high-quality photonic pigments that maintain the structural integrity and crystal characteristics even after removing the magnetic field, making it possible to use these anisotropic pigments for characterization and practical applications. Figure S1c,d, Supporting Information, shows two different projections of the photonic pigments with centered rectangular and rectangular symmetries, respectively. Figure S1c, Supporting Information, demonstrates a highly porous superlattice largely due to offset packing of the nanorods, which, combined with Figure S1d, Supporting Information, reveals the perfect structural order and crystallinity. The successful silica coating is evidenced by the intact crystal structures. The binding of adjoining nanorods prevents the crystals from being ruined by the capillary force during solvent evaporation (Figure S2a, Supporting Information). The high-magnification scanning electron microscopy (SEM) image in Figure S2b, Supporting Information, demonstrates the porous nature of the photonic crystals, with alternating anisotropic pores and well-aligned nanorods. To acquire more crystallographic information of this photonic pigment, we performed electron tomography and obtained 3D crystal structure through volume rendering of a series of 2D TEM projections (Figure 1d). The projection in the left panel of Figure 1e produces the same pattern as Figure S1c, Supporting Information, with the centered rectangular 2D lattice mapped on the TEM image. Interestingly, this projection evolves to a rectangular 2D lattice (right panel in Figure 1e) when the 3D volume rendering rotates 45°, with the mapped lattice symmetry being identical to the one in Figure S1d, Supporting Information. This experimental observation (Video S1, Supporting Information) suggests that these two highly related lattices come from colloidal crystal projections of (110) and (100) facets along <110> and <100> crystal directions, respectively. Another structural analysis that could benefit from electron tomography is the direct observation of transverse crystal symmetry by acquiring a horizontal cross-section of the 3D volume rendering. As shown in Figure 1f, we observe a square 2D lattice in this crystal plane rather than the hexagonal lattice often observed in colloidal assemblies featuring close packing. This important evidence implies that magnetic nanorods in the photonic pigments do not favor close packing, despite the hard contact of their surfaces. The square transverse symmetry also demonstrates the extraordinary rod packing along the <001> crystal directions, which in combination with rod packing in the other two crystal directions suggests a body-centered-tetragonal crystal. The projection schemes of the three typical facets, as shown in Figure 1g, agree well with experimental observations, confirming the unique tetragonal crystal structures of the photonic pigments.

### 2.2. Magnetically Tuning the Structural Colors of the Photonic Pigments

Tuning the structural color is possible by carefully controlling silica thickness and crystal orientation. For example, using 38 nm silica nanoshells (Figure S3a, Supporting Information) produces photonic pigments with primary blue and green colors; the binary colors under the dark-field optical microscope are attributed to random crystal orientation (left panel in **Figure 2**a). Considering the different periodicity of (100) and (110) facets, one can distinguish the diffraction planes of the two colors based on Bragg's law. The diffraction from (110) facets occurs at a shorter wavelength than that from (100) facets, which is consistent with the blue (middle panel in Figure 2a) and green (right panel in Figure 2a) colors from (110) and (100) planes, respectively. Increasing silica thickness to 66 nm (TEM image shown in Figure S3b, Supporting Information) led to green and red colors (left panel in Figure 2b). TEM images of the assembled crystals in Figure S3c,d, Supporting Information, show similar crystal structures as nanorods with a thinner silica coating. Accordingly, the diffraction from (110) and (100) planes produces green (middle panel in Figure 2b) and red colors (right panel in Figure 2b). The high quality of the photonic pigments is demonstrated by the bright colors in Figure S4, Supporting Information, and the perfect crystallinity in the large-scale TEM image in Figure S5, Supporting Information. Besides, the two primary colors of photonic pigments with a given silica thickness reveal the crystal-orientation-dependent structural colors. As demonstrated in Figure 2c, a set of optical microscopy images shows the color changes from green to orange and red when the silica thickness increases from 38 to 66 nm. The simultaneous peak shift in Figure 2d from 545 to 695 nm indicates a gradually increasing periodicity with silica thickness. Another unique feature of these photonic pigments is their highly porous and interconnected channels, making the pigments very susceptible to surrounding dielectric changes. We observe remarkable, rapid, and reversible color changes (green to red) in a small piece of photonic pigment when the 3D superstructure wets and dries (Figure 2e, Video S2 and Figure S6, Supporting information). A 150 nm shift in diffraction was observed due to an increased refractive index from 1 (air) to 1.33 (water) in the pores (Figure 2f). We then examine the stability of the photonic pigments using different methods. Figure S7a–c, Supporting Information shows that the photonic pigments could well maintain their diffraction peak position and intensity after being stored for six months, demonstrating their excellent long-term stability. Besides, the as-made photonic pigments are responsive to a magnetic field, and their diffraction peaks remain unchanged. In another experiment, we agitated the dispersion of photonic pigments in a vortex mixer for one week and measured their reflection spectra every two days. The resulting spectra in Figure S7d, Supporting

 

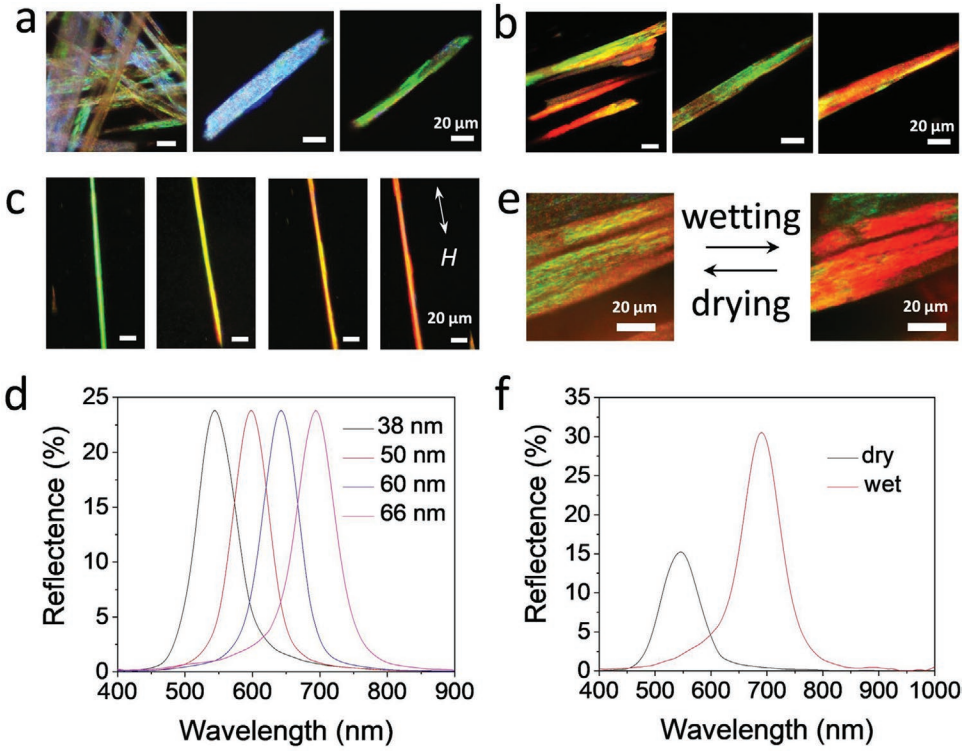


**Figure 2.** a,b) Dark-field optical microscopy images of the photonic pigments produced by magnetic assembly of $Fe_3O_4$@$SiO_2$ nanorods with the silica shell thickness of 38 nm (a) and 66 nm (b). The three images in (a,b) exhibit the photonic pigments with random orientations (left) and alignment along <110> (middle) and <100> (right) directions (relative to the image plane). c) Dark-field optical microscopy images of the photonic crystals with the silica thickness gradually increasing from 38 to 50, 60, and 66 nm from left to right. The white arrow indicates the magnetic field direction. d) The corresponding reflection spectra of the assembled crystals from nanorods with different silica thicknesses. e,f) Dark-field optical microscopy images (e) and the reflection spectra (f) of a crystal upon wetting by water and drying in air.

Information, shows negligible peak shift and intensity change, suggesting no degradation of the crystal structures.

The crystal fixation can be easily scaled up for mass production of high-quality, widely tunable photonic pigments. A series of digital pictures in **Figure 3**a shows three aqueous dispersions of photonic pigments made of magnetic nanorods with 38 nm, 50 nm, and 66 nm silica shells. In the absence of a magnetic field, each sample displays sparkles of mixed colors of individual pigments due to their random orientations, with blue and green for 38 nm sample (Video S3, Supporting information), blue, green, and yellow for 50 nm sample (Video S4, Supporting Information), and yellow and red for 66 nm sample (Video S5, Supporting Information). In a fixed magnetic field, each colloidal dispersion showed monochromatic structural colors due to the uniform alignment of all the pigments. When the field direction increased from 0° to 15° and 30°, the color changed from purple to blue and green for the 38 nm sample, blue to green and yellow for the 50 nm sample, and cyan to yellow and red for the 66 nm sample, respectively. These observations demonstrate the easy tuning of optical diffraction by magnetic fields and thus the widely accessible structural colors. Switching the field gradually from 0° to 90° changes the crystal from lateral to longitudinal orientations, leading to increased periodicity and redshift of the observed colors. At 90°, the structure colors in the three samples disappeared because the large periodicity along the <001> crystallographic direction shifts the diffraction peak to near-infrared regions (see Table S1, Supporting Information for summarized periodicity). A careful measurement reveals a shift from 360 to 580 nm (Figure 3b) and 500 to 680 nm (Figure 3c) for 38 and 66 nm samples, respectively.

### 2.3. Precise Magnetic Orientation Control

These observations underpin the important role of magnetic orientation control in creating multiple structural colors. We further performed synchrotron-based small-angle X-ray scattering (SAXS) measurement to characterize the collective alignment of pigments under a magnetic field (**Figure 4**a).[29] The acquired pattern in Figure 4b has a centered rectangular symmetry under a vertical magnetic field. This reciprocal lattice corresponds to the X-ray diffraction of the (110) facets. This evidence identifies the exposed (110) facets when a perpendicular magnetic field is applied relative to light incident direction, and therefore it is highly possible that the crystals in Figures 1c, 3a (at 0°), and **5**a also exhibit their (110) facets. Switching the magnetic field from the perpendicular to parallel direction relative to incident light produces an interesting square lattice (Figure 4c) that demonstrates the change of the diffraction from <110> to <001> crystal directions. One measurable consequence of this event is the increase in periodicity along the light

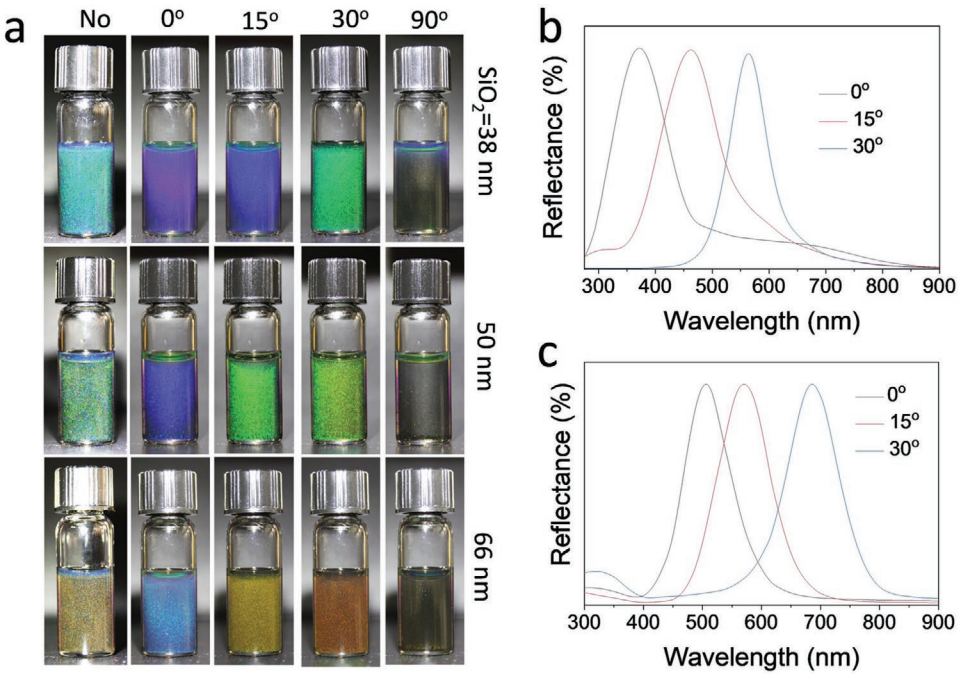


**Figure 3.** a) Digital pictures of the dispersions of photonic pigments under magnetic fields of varying directions. b,c) The reflection spectra of crystals aligned under magnetic fields of different directions. The silica shell thickness is 38 nm in (b) and 66 nm in (c).

incidence and the corresponding redshift of diffraction. A linear profile of the diffraction patterns of (110) facets, obtained under a vertical magnetic field, is plotted in Figure 4d, exhibiting several characteristic peaks in the measured $q$ range with position ratios ($q_n/q_1$, where $q_n$ refers to the $n$th peak) of 1, 2, 3, 4, 6, and 9. Based on these diffraction peaks, the periodicity between (110) crystal planes is calculated as 144.035 nm (Table S1, Supporting Information). Figure 4e shows a few representative linear profiles of the SAXS patterns measured under a horizontal magnetic field. The defined peaks are detectable even in

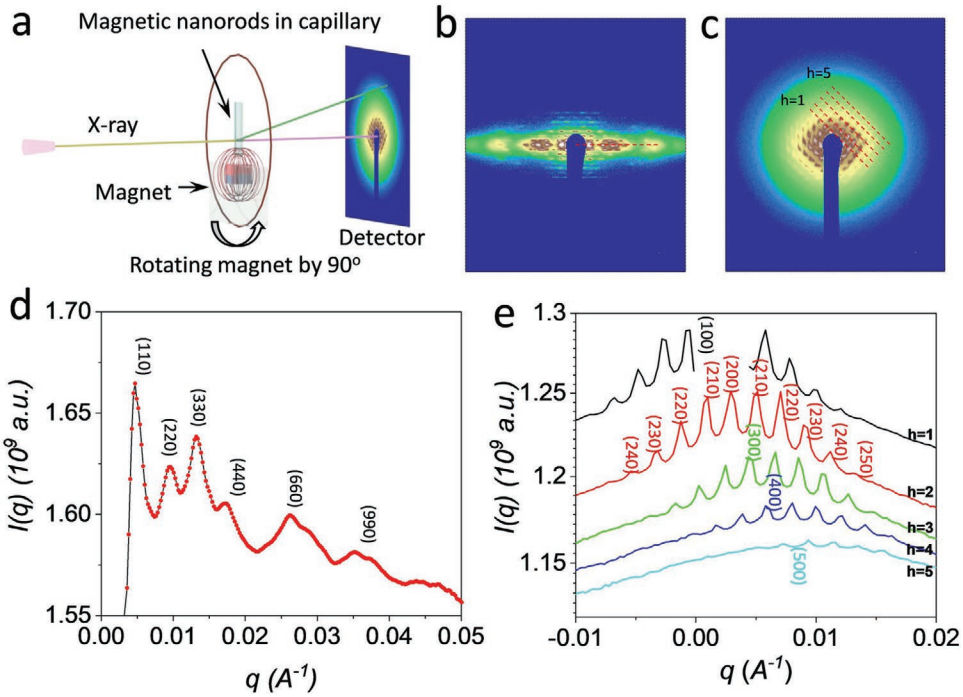


**Figure 4.** SAXS measurement of the photonic crystals. a) Schematic illustration of the setup. b,c) SAXS patterns of the crystals under a vertical (b) and horizontal magnetic field (c). d,e) Linear profile of the scattering patterns under a vertical (d) and horizontal magnetic field (e).

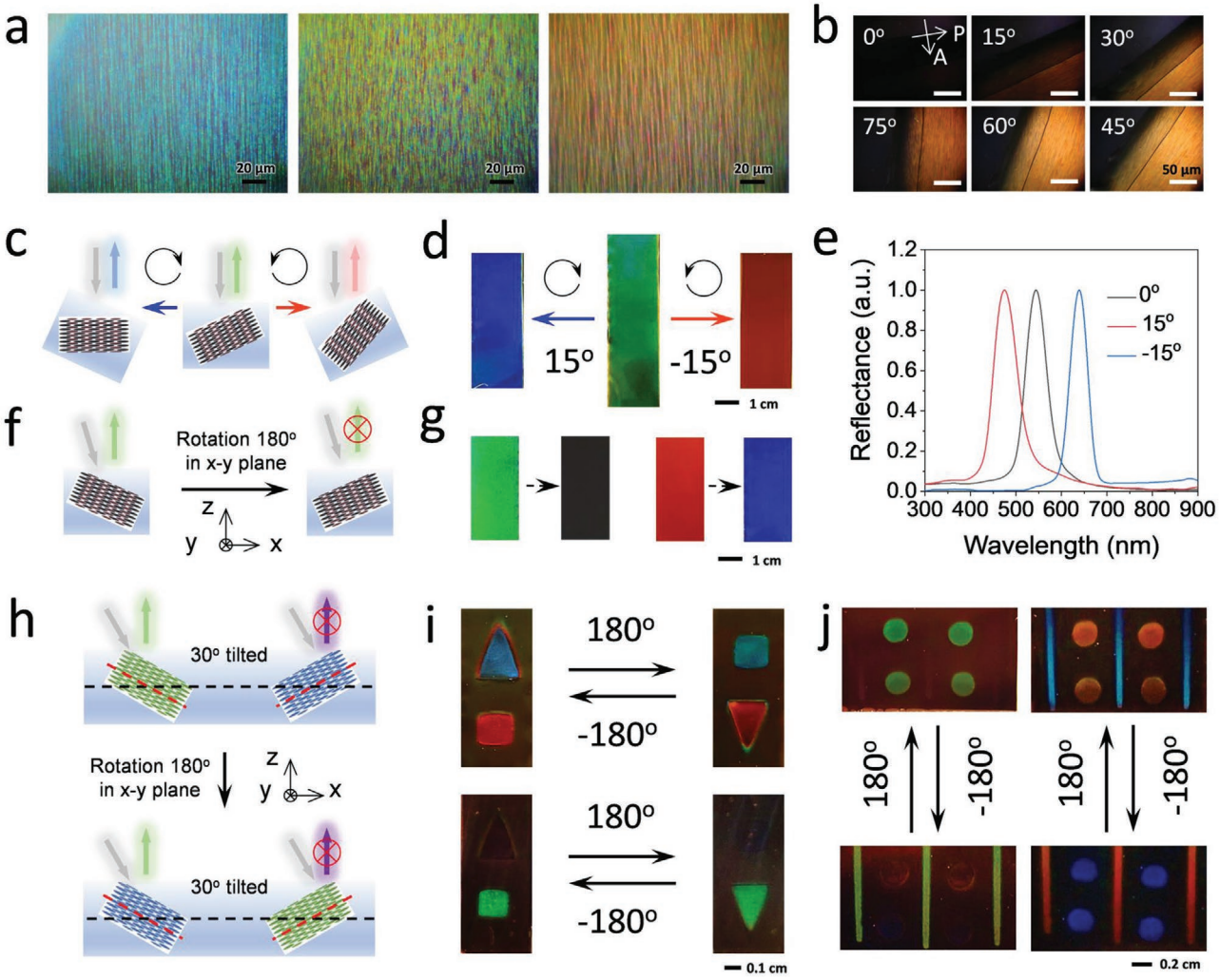


**Figure 5.** Highly tunable multicolor photonic pigments for rotation-asymmetric mechanochromic photonic devices. a) Dark-field microscopy images of the photonic pigments aligned along different directions in photonic films. b) Polarized microscopy images of the photonic films under different rotation angles. The directions of the polarizer (P) and analyzer (A) are shown in white arrows. The angle between the rod alignment and the polarizer direction is also labeled in each image. c) Schematic illustration of the rotation-asymmetric photonic film by magnetically aligning the photonic pigments along a pre-designed direction. d) Digital photos showing the color changes of the photonic film in response to clockwise and counterclockwise rotation. e) The corresponding reflection spectra of the film during the opposite rotation. f) Schematic illustration of changes in the incident angle and structural colors of the photonic film during rotation by 180° in the *x*–*y* plane. g) Digital photos of photonic films before and after rotation. The photonic pigments are aligned along 30° to the film surface. The incident angle in the left and right panels is 30° and 40°, respectively. h) Schematic illustration of the alignment of the photonic pigments in the solid film for emerging mechanochromic responses. i,j) Digital photos of two photonic films showing the displayed patterns and their color changes in response to mechanical rotation. The incident angle is 40° in the top panel of (i) and right panel of (j), while it is 30° in the other two panels. The positive and negative angles represent clockwise and counterclockwise mechanical rotation, respectively.

the fifth order, which, together with the ninth diffraction peak in the vertical configuration, validates the high uniformity and perfect crystallinity of the photonic pigments. It is worth highlighting that the efficient orientation control is enabled by the magnetic anisotropy of the $Fe_3O_4$ nanorods, making the long axes of both the constituent nanorods and the photonic pigments parallel to the external magnetic field.[30]

### 2.4. Rotation-Asymetric Mechanochromic Devices

By taking advantage of the efficient magnetic alignment of anisotropic pigments, we further develop rotation-asymmetric photonic devices that can exhibit dynamic color-switching or display distinct patterns in response to mechanical rotation. This unconventional optical device is achieved by magnetically aligning the photonic pigments in a photocurable polymer film and fixing their orientation in different color domains. When a horizontal magnetic field was used during photopolymerization (Figure S8a, Supporting Information), the photonic pigments in the polymer matrix exhibited a uniform blue color (Figure 5a). Increasing the magnetic field orientation relative to the film surface led to a color change to green and red due to increased periodicity (Figure S8b,c, Supporting Information). For horizontal alignment, the unidirectional in-plane crystal orientation was also demonstrated by the apparent birefringence in the photonic

film, which has orientation-dependent transmittance under two cross polarizers (Figure 5b). When the pigment orientation was parallel to the polarizer or analyzer (at 0°), the film became dark due to the low transmittance of light. At 45°, the film appeared brightest, indicating the highest transmittance (Video S6, Supporting Information). These optical effects demonstrate the good alignment of the photonic pigments to the applied magnetic field. In conventional opal and inverse opal pigments, their responses to viewing angle changes are symmetric due to the high crystal symmetry. Our anisotropically structured photonic pigments can break this limitation by carefully controlling the crystal orientation in the polymer film. We introduced a magnetic field-assisted polymerization method to create photonic films with designated images. As shown in Figure S9, Supporting Information, a magnetic field was applied during each ultraviolet (UV) exposure so that photonic crystals were fixed in a proper direction for color generation. Figure 5c illustrates the tilted alignment of the photonic pigments in the solid film and their re-alignment upon rotation. Because the photonic pigments were magnetically aligned along a pre-designed direction, clockwise and counterclockwise rotation decreased and increased the angle between the long axis of the photonic crystals and incident direction of light, leading to opposite blueshift and redshift of the structural colors, respectively (Figure 5d,e). If the film was rotated in the *x*–*y* plane, it exhibited interesting on–off switching of the structural colors. As shown in Figure 5f, this in-plane rotation changed the light incident angle because of the tilted crystal alignment, making the diffraction peaks shift out of the visible spectrum. The onset of this principle can display distinct visual effects depending on initial incident angles. As shown in the left panels (incident angle = 30°) of Figure 5g, the initial green color of a photonic film made by unidirectional alignment of pigments (≈30° to film surface) disappeared due to the rotation-induced decrease in incident angle and the ensuing blueshift of the diffraction peak to the UV. When the incident angle increased to 40°, the film appeared red uniformly, which changed to blue during the same rotation in the *x*–*y* plane (right panel in Figure 5g). The concept underlying this optical transition is the rotation-induced change of the incident angle, which is enabled by and unique to the anisotropic photonic pigments. To demonstrate potential applications of this concept, we developed photonic films by patterning the pigments along pre-designed directions in each domain (represented by blue and green crystals in the right and left parts of the scheme in Figure 5h, respectively) by sequential polymerization of the film under the presence of a photomask. The photonic pigments in the two domains were aligned symmetrically, with the same tilting angle (≈30°) to the film surface in opposite tilting directions (Figure 5h). Rotating such a patterned photonic film in the *x*–*y* plane led to two distinct visual effects depending on the incident angle. When the incident angle was ≈40°, the top "triangle" domain appeared blue, while the bottom "square" domain exhibited red because of the tilting-induced variation in incident angles. Simply rotating the film by 180° in the *x*–y plane led to color switching in the two domains due to the changes in their incident geometry (top panels in Figure 5i; Video S7, Supporting Information). If the incident angle decreased to 30°, the diffraction in the two domains would blueshift, with red "square" changing to green and blue "triangle" disappearing due to the shift of its photonic bandgap to the UV region (Figure S10a,b, Supporting Information). Interestingly, rotating such a film by 180° in the *x*–*y* plane changed the shape of the perceived pattern from a "square" to a "triangle," which was caused by switching the two domains (bottom panels in Figure 5i). In another design, a photonic film was prepared based on the same concept to display distinct images. As demonstrated in the left panels of Figure 5j, the observed patterns changed from a 2D matrix of circles to a 1D linear array upon 180° rotation. If the incident angle increased to 40° (Figure S10c, Supporting Information), the two encrypted images could be simultaneously observed with red and blue colors in each domain, and their colors switched during rotation (Video S8, Supporting Information). Realizing other color switching is also possible through changing the tilting angle or incident angle. For example, decreasing the incident angle to 20° further blueshifts the diffraction peaks, leading to optical switching between blue and no color during rotation (Figure S11a, Supporting Information). It is important to point out that this strategy can be used to print arbitrary images with desirable color-switching by carefully controlling the tilting and incident angles (Figure S11b, Supporting Information). The programmable optical performance underpins the importance of orientational control over the current photonic pigments in developing advanced optical devices. For example, these rotation-asymmetric photonic films can be attached to flat and curved surfaces, and their unique color switching in response to mechanical rotation can be used for anti-counterfeiting purposes (Figure S12, Supporting Information).

## 3. Conclusion

We have developed photonic pigments by the magnetic assembly of $Fe_3O_4$@$SiO_2$ nanorods, which can produce multiple colors in response to the varying magnetic field direction. The magnetic shape anisotropy of nanorods induces the preferred offset rod packing, producing tetragonal crystals featuring hard contact, anisotropic non-close-packing, and well-defined and interconnected channels. Due to their non-close-packing nature, the photonic pigments contain large pores for accommodating fast and sensitive colorimetric responses to surrounding dielectric changes. More importantly, the structural and magnetic anisotropy of the photonic pigments enables precise orientation control using magnetic means so that they can be easily aligned along pre-designed directions for desirable structural colors and further produce patterned photonic films. These unique features enable the design and fabrication of rotation-asymmetric photonic devices that can exhibit dynamic color-switching or display varying patterns and encrypted information upon rotation. As the materials synthesis is highly scalable and the magnetic assembly is straightforward and robust, our photonic pigments hold great promise for creating many advanced optical devices, including colorimetric sensors, anti-counterfeiting devices, and multicolor passive photonic displays.

## Supporting Information

Supporting Information is available from the Wiley Online Library or from the author.

 

## Acknowledgements

The authors are grateful for the financial support from the U.S. National Science Foundation (CHE-1808788). The electron tomography work done at UCI is supported by the U.S. National Science Foundation (CHE-1900401). This research used resources of the Center for Functional Nanomaterials, which is a U.S. DOE Office of Science Facility, at Brookhaven National Laboratory under Contract No. DE-SC0012704. This research used beamline 7.3.3 of the Advanced Light Source, which is a DOE Office of Science User Facility under contract no. DE-AC02-05CH11231. Acknowledgment is also made to the Central Facility for Advanced Microscopy and Microanalysis at UCR for help with TEM analysis.

## Conflict of Interest

The authors declare no conflict of interest.

## Data Availability Statement

The data that support the findings of this study are available from the corresponding author upon reasonable request.

## Keywords

magnetic assembly, mechanochromic devices, orientational control, photonic crystals, photonic pigments, structural color

Received: September 16, 2021
Revised: October 17, 2021
Published online: December 2, 2021

[1] a) J. D. Joannopoulos, P. R. Villeneuve, S. Fan, *Nature* **1997**, *386*, 143; b) J. H. Moon, S. Yang, *Chem. Rev.* **2010**, *110*, 547.
[2] a) Y. Zhao, Z. Xie, H. Gu, C. Zhu, Z. Gu, *Chem. Soc. Rev.* **2012**, *41*, 3297; b) Z. Li, Y. Yin, *Adv. Mater.* **2019**, *31*, 1807061.
[3] J. Ge, Y. Yin, *Angew. Chem., Int. Ed.* **2011**, *50*, 1492.
[4] H. Li, C. Li, W. Sun, Y. Wang, W. Hua, J. Liu, S. Zhang, Z. Chen, S. Wang, Z. Wu, *Adv. Mater.* **2019**, *31*, 1900388.
[5] R. D. Meade, A. Rappe, K. Brommer, J. Joannopoulos, O. Alerhand, *Phys. Rev. B* **1993**, *48*, 8434.
[6] a) J. Wang, Y. Zhang, S. Wang, Y. Song, L. Jiang, *Acc. Chem. Res.* **2011**, *44*, 405; b) S. Takahashi, K. Suzuki, M. Okano, M. Imada, T. Nakamori, Y. Ota, K. Ishizaki, S. Noda, *Nat. Mater.* **2009**, *8*, 721; c) D. Liu, F. Zhou, C. Li, T. Zhang, H. Zhang, W. Cai, Y. Li, *Angew. Chem., Int. Ed.* **2015**, *54*, 9596.
[7] a) Z. Cai, Z. Li, S. Ravaine, M. He, Y. Song, Y. Yin, H. Zheng, J. Teng, A. Zhang, *Chem. Soc. Rev.* **2021**, *50*, 5898; b) G. von Freymann, V. Kitaev, B. V. Lotsch, G. A. Ozin, *Chem. Soc. Rev.* **2013**, *42*, 2528; c) D. V. Talapin, J.-S. Lee, M. V. Kovalenko, E. V. Shevchenko, *Chem. Rev.* **2010**, *110*, 389.
[8] E. S. Goerlitzer, R. N. Klupp Taylor, N. Vogel, *Adv. Mater.* **2018**, *30*, 1706654.
[9] Y. Wang, H. Cui, Q. Zhao, X. Du, *Matter* **2019**, *1*, 626.
[10] J. G. Park, S. H. Kim, S. Magkiriadou, T. M. Choi, Y. S. Kim, V. N. Manoharan, *Angew. Chem., Int. Ed.* **2014**, *53*, 2899.
[11] a) H. S. Lee, J. H. Kim, J. S. Lee, J. Y. Sim, J. Y. Seo, Y. K. Oh, S. M. Yang, S. H. Kim, *Adv. Mater.* **2014**, *26*, 5801; b) F. Fu, L. Shang, Z. Chen, Y. Yu, Y. Zhao, *Sci. Rob.* **2018**, *3*, eaar8580.
[12] a) L. Shang, W. Zhang, K. Xu, Y. Zhao, *Mater. Horiz.* **2019**, *6*, 945; b) W. Hong, Z. Yuan, X. Chen, *Small* **2020**, *16*, 1907626; c) R. Vaz, M. F. Frasco, M. G. F. Sales, *Nanoscale Adv.* **2020**, *2*, 5106.
[13] M. Wang, L. He, W. Xu, X. Wang, Y. Yin, *Angew. Chem., Int. Ed.* **2015**, *54*, 7077.
[14] a) A. M. Brozell, M. A. Muha, A. N. Parikh, *Langmuir* **2005**, *21*, 11588; b) D. Liu, R. Aleisa, Z. Cai, Y. Li, Y. Yin, *Matter* **2021**, *4*, 927; c) J. H. Moon, G. R. Yi, S. M. Yang, D. J. Pine, S. B. Park, *Adv. Mater.* **2004**, *16*, 605; d) W. Han, Z. Lin, *Angew. Chem., Int. Ed.* **2012**, *51*, 1534.
[15] a) S.-H. Kim, J.-G. Park, T. M. Choi, V. N. Manoharan, D. A. Weitz, *Nat. Commun.* **2014**, *5*, 3068; b) L. Shang, Y. Cheng, Y. Zhao, *Chem. Rev.* **2017**, *117*, 7964; c) Y. Zhao, Y. Cheng, L. Shang, J. Wang, Z. Xie, Z. Gu, *Small* **2015**, *11*, 151; d) M. Xiao, Z. Hu, Z. Wang, Y. Li, A. D. Tormo, N. Le Thomas, B. Wang, N. C. Gianneschi, M. D. Shawkey, A. Dhinojwala, *Sci. Adv.* **2017**, *3*, e1701151; e) T. M. Choi, J.-G. Park, Y.-S. Kim, V. N. Manoharan, S.-H. Kim, *Chem. Mater.* **2015**, *27*, 1014.
[16] a) C. García Núñez, W. T. Navaraj, F. Liu, D. Shakthivel, R. Dahiya, *ACS Appl. Mater. Interfaces* **2018**, *10*, 3058; b) D. Xia, A. Biswas, D. Li, S. R. Brueck, *Adv. Mater.* **2004**, *16*, 1427; c) H. Yang, P. Jiang, *Langmuir* **2010**, *26*, 13173.
[17] a) A. C. Arsenault, D. P. Puzzo, I. Manners, G. A. Ozin, *Nat. Photonics* **2007**, *1*, 468; b) J. Hou, M. Li, Y. Song, *Angew. Chem., Int. Ed.* **2018**, *57*, 2544.
[18] a) J. Wang, L. Wang, Y. Song, L. Jiang, *J. Mater. Chem. C* **2013**, *1*, 6048; b) R. Shanker, S. Sardar, S. Chen, S. Gamage, S. Rossi, M. P. Jonsson, *Nano Lett.* **2020**, *20*, 7243; c) W. Li, Y. Wang, M. Li, L. P. Garbarini, F. G. Omenetto, *Adv. Mater.* **2019**, *31*, 1901036.
[19] a) B. M. Boyle, T. A. French, R. M. Pearson, B. G. McCarthy, G. M. Miyake, *ACS Nano* **2017**, *11*, 3052; b) S. Liu, Y. Yang, L. Zhang, J. Xu, J. Zhu, *J. Mater. Chem. C* **2020**, *8*, 16633.
[20] a) Y. Zhao, Z. Xie, H. Gu, L. Jin, X. Zhao, B. Wang, Z. Gu, *NPG Asia Mater.* **2012**, *4*, e25; b) Y. Zhao, L. Shang, Y. Cheng, Z. Gu, *Acc. Chem. Res.* **2014**, *47*, 3632; c) R. C. Schroden, M. Al-Daous, C. F. Blanford, A. Stein, *Chem. Mater.* **2002**, *14*, 3305.
[21] H. Kim, J. Ge, J. Kim, S.-e. Choi, H. Lee, H. Lee, W. Park, Y. Yin, S. Kwon, *Nat. Photonics* **2009**, *3*, 534.
[22] Z. Li, F. Yang, Y. Yin, *Adv. Funct. Mater.* **2020**, *30*, 1903467.
[23] W. Xu, Z. Li, Y. Yin, *Small* **2018**, *14*, 1801083.
[24] a) C. Li, Y. Yu, L. Wang, S. Zhang, J. Liu, J. Zhang, A.-B. Xu, Z. Wu, J. Tong, S. Wang, *Chem. Mater.* **2019**, *31*, 9513; b) Y. Yin, A. P. Alivisatos, *Nature* **2005**, *437*, 664; c) C. Li, S. Zhang, B. Zhang, J. Liu, W. Zhang, A. A. Solovev, R. Tang, F. Bao, J. Yu, Q. Zhang, *Angew. Chem., Int. Ed.* **2018**, *57*, 3772; d) X. Pang, Y. He, J. Jung, Z. Lin, *Science* **2016**, *353*, 1268.
[25] C. Zhang, Z. Wu, Z. Chen, L. Pan, J. Li, M. Xiao, L. Wang, H. Li, Z. Huang, A.-B. Xu, *J. Mater. Chem. C* **2020**, *8*, 16067.
[26] a) Z. Li, J. Jin, F. Yang, N. Song, Y. Yin, *Nat. Commun.* **2020**, *11*, 1; b) W. Xu, M. Wang, Z. Li, X. Wang, Y. Wang, M. Xing, Y. Yin, *Nano Lett.* **2017**, *17*, 2713; c) Z. Li, M. Wang, X. Zhang, D. Wang, W. Xu, Y. Yin, *Nano Lett.* **2019**, *19*, 6673.
[27] a) L. He, M. Wang, J. Ge, Y. Yin, *Acc. Chem. Res.* **2012**, *45*, 1431; b) Z. Li, C. Qian, W. Xu, C. Zhu, Y. Yin, *Sci. Adv.* **2021**, *7*, eabh1289.
[28] Y. Hu, L. He, Y. Yin, *Angew. Chem., Int. Ed.* **2011**, *50*, 3747.
[29] K. Deng, X. Huang, Y. Liu, L. Xu, R. Li, J. Tang, Q.-l. Lei, R. Ni, C. Li, Y. S. Zhao, *Nano Lett.* **2020**, *20*, 7367.
[30] a) M. Wang, C. Gao, L. He, Q. Lu, J. Zhang, C. Tang, S. Zorba, Y. Yin, *J. Am. Chem. Soc.* **2013**, *135*, 15302; b) Z. Li, J. Zhang, J. Jin, F. Yang, R. Aleisa, Y. Yin, *J. Am. Chem. Soc.* **2021**, *143*, 15791.